Characterizing Emerging Cell Chemistries for Battery Energy Storage Systems

Prepared for the

U.S. Department of Energy
Office of Electricity Delivery and Energy Reliability

Under Cooperative Agreement No. DE-EE0003507
Hawai‘i Energy Sustainability Program

Task 3.2.4 Report on Emerging Cell Chemistries

By the

Hawai‘i Natural Energy Institute
School of Ocean and Earth Science and Technology
University of Hawai‘i

May 2016

Acknowledgement: This material is based upon work supported by the United States Department of Energy under Award Number DE-EE0003507-06NT42847 and by ONR Hawaii Energy and Environmental Technologies (HEET) 2010 Initiative, award No N00014-11-1-0391.

Table of Contents

EXECUTIVE SUMMARY

The Hawai‘i Energy Sustainability Program (HESP) project objectives under subtask 3.2 comprise testing battery storage systems for management of intermittency of renewable generation on the power grid. These testing and prognosis efforts support the aggressive goals of the Hawai‘i Clean Energy Initiative, to facilitate reduced use of fossil fuels in Hawai‘i. This work was closely coordinated with a similar BESS program under Hawai‘i Natural Energy Institute’s (HNEI’s) ONR funded Hawaii Energy and Environmental Technologies (HEET) 2010 Initiative, award No N00014-11-1-0391. In order to provide the best possible comparison of the tested technologies, all the tested cells will be described in this report.

Emerging lithium-ion battery technologies offer potentially improved cost, safety, cycle life and performance, but little information is available regarding the degradation pace of these battery systems. It is therefore critical to evaluate these cell chemistries and designs before selecting a lithium-ion technology for a large scale battery energy storage system intended to last for over 10 years. This report presents a comparison of the long-term performance of four different cells with different materials: one lithium titanate oxide (LTO) based cell from Altairnano, tested under ONR funding, and three graphite based cells from SAFT America, tested under DOE funding.

As part of the initial testing, the manufacturing quality of the cells was assessed by characterizing the cell-to-cell variations. Because large scale battery energy storage systems typically consist of thousands of cells, cell-to-cell variations can be detrimental to the overall performance of the battery system. Overall, we found these large format cells to offer noticeable but acceptable cell-to-cell variations.

Continuous cycle-aging was undertaken for a year and a half, reaching over 1000 cycles by the end of the project. Results revealed that the cells with a graphitic negative electrode degraded far more than the cell with the alternative LTO negative electrode. Results also indicated that the positive electrode material and the electrode design influence the degradation’s mechanism and pace, but to a lesser extent. SAFT positive electrodes tested included iron phosphate (LFP), and two nickel cobalt aluminum (NCA) electrodes, one high-power and the other high-energy cell designs.

At the thousand test cycles mark, the LTO based cell from Altairnano demonstrated excellent performance with less than 1% capacity loss. The graphite based cells from SAFT exhibited less attractive performances: the LFP based cell suffered from 7% capacity loss, the high-power NCA based cell lost 19% of its initial capacity and the high-energy NCA based cell lost the most capacity, 37%.

For each chemistry, a detailed quantitative analysis of the degradation mechanisms was carried out using HNEI’s unique battery diagnosis capabilities. Variations in observed capacity retention were tied to the differences in degradation mechanisms between chemistries. In particular, the LTO based cell has been found to be less prone to loss of lithium inventory than graphite based cells, which explains its very good capacity retention.

Finally, using HNEI's diagnostic methods, the longer term capacity retentions of all four cells were forecast. The prognoses showed that the LTO based and LFP based cells should be able to withstand more than 8000 cycles before reaching the end of life criterion, and thus could be of interest for battery storage systems. The two other cells, NCA based, have been predicted to fail much earlier.

INTRODUCTION

This report addresses subtask 3.2.3, the characterization of emerging cell chemistries. In this subtask, 3 types of commercial Lithium-ion (Li-ion) batteries of emerging chemistries were evaluated and the study has been concluded as planned. Additionally, a fourth type of commercial Li-ion cell was tested under funding from ONR. This evaluation has generated useful information to allow us to assess the cell life performance for battery energy storage system (BESS) applications scoped for this project. To provide the best comparison of the results, the testing of the 4 types of cells will be described in this report. The characteristics and specifications published by the manufacturers are listed in Table 1.

As showcased in Table 1, the selected cells contain 3 different positive electrode materials: NMC, NCA and LFP (see note below Table 1 for details). NMC and NCA materials are an evolution of $LiCoO_2$ (LCO) which is the conventional positive electrode material that is used in batteries for most portable electronics to date. NCA and NMC chemistries were developed in recent years to improve on the performance of LCO electrodes while reducing the cobalt content, cobalt being expensive and toxic. The LFP chemistry is based on a different structural framework, the olivine structure, and offers the advantage of being able to intercalate/deintercalate lithium ions at a higher pace, making it an ideal candidate for high power applications despite its slightly lower voltage (see nominal voltage in Table 1). This type of chemistry is already widely adopted in power tool applications.

Table 1. Specifications and characteristics of the four commercial cell types tested in this work.

Cell Model	Vendor	Format	Chemistry	Rated Capacity (Ah)	Nominal Voltage (V)	Specific Energy (Wh/kg)	Specific Power (kW/kg)	Funding Source
VL12V	Saft America (SA)	Cylindrical	PE: NCA NE: Graphite	14	3.65	80	6.6	DOE
VL52E	Saft America (SA)	Cylindrical	PE: NCA NE: Graphite	52	3.6	185	0.2	DOE
VL10VFe	Saft America (SA)	Cylindrical	PE: LFP NE: Graphite	10	3.3	55	5	DOE
ALT nLTO	Altairnano (ALT)	Pouch	PE: NMC NE: LTO	13	2.2	74	1.6	ONR

Note:
NMC — Positive electrode (or PE) materials with a nominal composition of $Li(Ni_XMn_YCo_Z)O_2$.
LTO — Negative electrode (or NE) materials with a nominal composition of $Li_4Ti_5O_{12}$.
NCA — Positive electrode materials with a nominal composition of $Li(Ni_XCo_YAl_Z)O_2$.
LFP — Positive electrode materials with a nominal composition of $LiFePO_4$.

Looking at the negative electrode, the selected cells contain 2 different materials: graphite and LTO. Graphite is by far the most commonly used negative electrode material for Li-ion batteries today. It offers a combination of a large specific capacity and a low intercalation potential. This makes graphite the most interesting viable negative electrode to date for energy density considerations. In contrast, the "benchmark" metallic lithium electrode has safety drawbacks. The drawback of the low intercalation potential of lithium-ions into graphite is that the cell is operating below the electrolyte's thermodynamic stability window. As a result, we typically observe a formation of passivation layers that gradually reduce the capacity retention of the cells. In comparison, LTO has a higher intercalation potential which lies within the electrolyte's stability window. This higher intercalation potential makes the LTO based cells almost immune to passivation layers while negatively impacting the cell's energy density resulting from a significantly lower nominal cell voltage (e.g. 2.2V in Table 1).
The ALT nLTO chemistry was the one selected for installation in the COASTAL BESS supervised by HNEI. It is therefore of interest to compare its degradation to the other high quality batteries provided by SAFT America.

INITIAL CONDITIONING AND CHARACTERIZATION TEST

Before starting the cycle life evaluation, the four different cell types were compared using three critical parameters that can be indicators of cell performance for high-power applications in grid energy storage. Because BESS systems are made of several hundred cells connected together, it is imperative for the cells to have little cell-to-cell variations to ensure optimal long term performance and safety. Our initial conditioning and characterization test (ICCT) is meant to assess these cell-to-cell variations and consists of several cycles at C/2 (discharge in 2 hours) until the capacity of the cell is stable within 0.2% then 2 additional cycles at C/2 and C/5 (discharge in 5 hours) with 4 hours rest before and after the discharges. All charges are performed using the manufacturer recommended conditions. The capacities as well as the rest cell voltages (RCV) measured during the final part of the ICCT are used to calculate the three parameters that are critical in determining the manufacturing variability in a batch of cells: the rate capability, the capacity ration and the resistance [1].

Rate capability [unit-less] – The rate capability represents the cell's ability to deliver stored capacity when the discharge rate increases. In this study, it was calculated by dividing the capacity obtained at C/2 by the capacity at C/5.

Capacity ration [mAh / %SOC] – The term "capacity ration" is the capacity (Ah) obtained for each one percent of the state of charge (SOC). It typically reflects the amount of active material in a cell. RCV measurements at the beginning of discharge (BOD) and the end of discharge (EOD) are used to derive a SOC range by interpolation of the maximum and minimum SOCs (e.g. 99.7 – 3.2 %). The capacity ration is then calculated by dividing the capacity returned during discharge by the SOC range variation.

1 M. Dubarry, N. Vuillaume and B. Y. Liaw, "Origins and accommodation of cell variations in Li-ion battery pack modeling"., *International Journal of Energy Research* 34(2), p.216 (2010),

Ohmic resistance [Ohm] – The ohmic resistance consists of the contact resistance of the cell in the circuit and the conductive resistance of the cell (which primarily comes from the electrolyte). It is calculated using the initial voltage drop associated with the C/2 and C/5 discharges.

For the ICCT, six ALT nLTO cells, and four of each of the SA VL12V cells, VL52E and VL10Fe cells were tested. For each cell type, the weights along with the aforementioned metrics are reported in Table 2 (mean value and standard deviation in parenthesis). An example of the results for the ALT nLTO cell is presented in Figure 1.

Table 2. Initial cell performance comparison.

	ALT nLTO	VL12V	VL52E	VL10VFe
Weight (g)	400.5 (± 0.1%)	628.4 (± 0.6%)	971.6 (± 0.4%)	602.3 (± 0.5%)
C/2 capacity (Ah)	14.74 (± 0.6%)	13.77 (± 1.8%)	52.20 (± 0.6%)	11.00 (± 2.7%)
C/5 capacity (Ah)	15.24 (± 0.7%)	13.96 (± 1.7%)	53.00 (± 0.6%)	11.08 (± 2.6%)
Rate capability	0.97 (± 0.8%)	0.99 (± 0.2%)	0.98 (± 0.2%)	0.99 (± 0.4%)
BOD RCV @ C/2 (V)	2.731 (± 0.2%)	4.090 (± 0.1%)	4.092 (± 0.0%)	3.463 (± 0.7%)
EOD RCV @ C/2 (V)	2.062 (± 0.8%)	3.162 (± 1.1%)	3.202 (± 0.4%)	2.851 (± 1.4%)
EOD SOC @ C/2 (%)	4.05 (± 0.6%)	2.393 (± 0.4%)	3.48 (± 0.2%)	1.20 (± 0.3%)
BOD RCV @ C/5 (V)	2.684 (± 0.3%)	4.092 (± 0.0%)	4.092 (± 0.0%)	3.463 (± 0.8%)
EOD RCV @ C/5 (V)	1.895 (± 1.9%)	2.980 (± 0.7%)	3.071 (± 0.3%)	2.771 (± 0.5%)
EOD SOC @ C/5 (%)	1.44 (± 0.3%)	0.91 (± 0.1%)	1.84 (± 0.1%)	0.68 (± 0.1%)
Resistance (mΩ)	9.51 (± 10%)	1.03 (± 6%)	1.58 (± 16%)	4.05 (± 51%)
Q ration (mAh.%SOC)	154.2 (± 0.6%)	146.9 (± 1.6%)	542.4 (± 0.6%)	111.7 (± 2.8%)

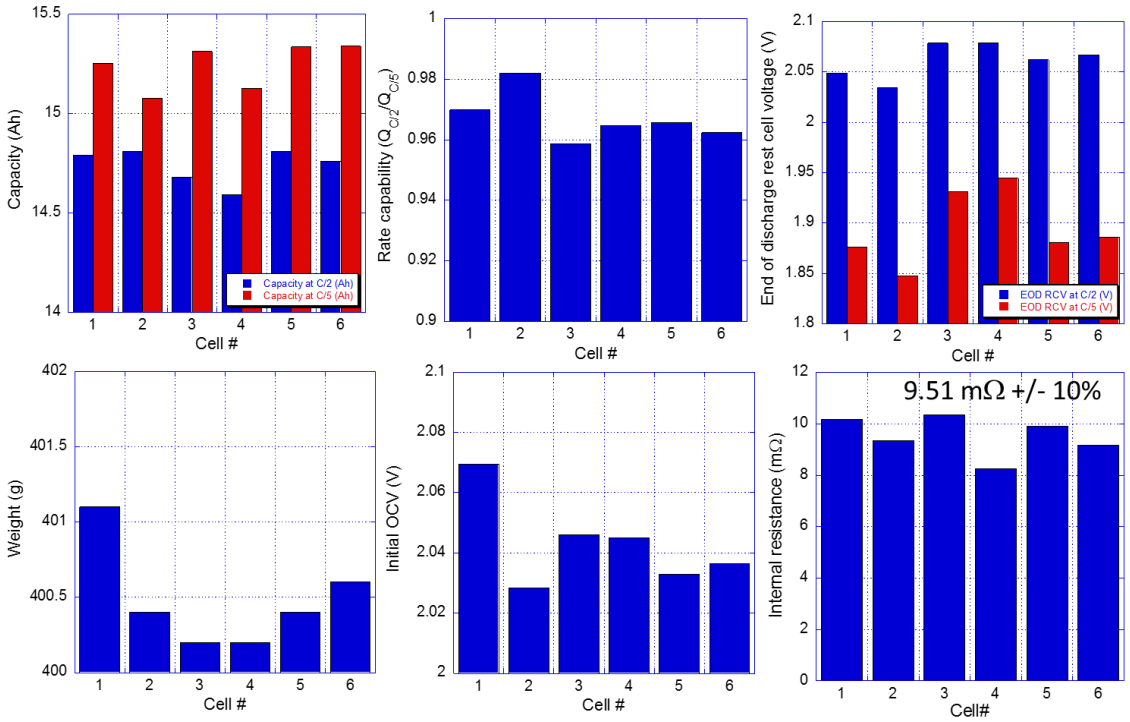

Figure 1: Results of the ICCT test for the ALT nLTO cell.

INITIAL CONDITIONING AND CHARACTERIATION TEST RESULTS

According to the ICCTs, the six ALT nLTO cells exhibited an average C/2 capacity ($Q_{C/2}$) of 14.742 ± 0.088 Ah and C/5 capacity ($Q_{C/5}$) 15.242 ± 0.113 Ah. The variation in capacity between cells is within 1%, which meets the expectation of current state-of-the-art (SOTA) performance requirements. The rate capability is 0.967 and the ohmic resistance variations are acceptable (i.e. ±10%). For the SA VL12V cells, the average capacity for C/2 is $Q_{C/2}$ = 13.77 ± 0.25 Ah and for C/5 $Q_{C/5}$ = 13.96 ± 0.24 Ah, which are close to the rated capacity. The rate capability is 0.986 and the ohmic resistance spread is small (i.e. ±6%).
Because of the larger capacity rating of the SA VL52E cells at 52 Ah, our testing equipment cannot use the C/2 and C/5 rates used in other tests. Instead, C/3 and C/7 (discharge in 3 and 7 hours respectively) were used to determine the C/3 capacity $Q_{C/3}$ = 52.20 ± 0.30 Ah (stand. dev. = 0.57%) and $Q_{C/7}$ = 53.00 ± 0.31 Ah (standard deviation = 0.59%), allowing measurement in line with the test channel range and accuracy desired. The rate capability is 0.985 and the ohmic resistance spread is acceptable (i.e. ±16%). Finally, for the SA VL10VFe, the average cell capacity at C/2 is about $Q_{C/2}$ = 11.00 Ah, with 2.73% deviation. This deviation is considerably higher than the other cells. The average C/5 capacity is $Q_{C/5}$ = 11.08 Ah with 2.58% deviation. The rate capability is 0.993, consistent with the high power design. The ohmic resistance spread is 51% which is of concern. It might be attributed to test holder variations or connection issues, not necessarily reflecting the internal ohmic resistance problem. It is unlikely a power cell design has such a wide range of variation with internal ohmic resistance. Overall, the cell to cell variations seem to be higher for this batch of cells. The high deviation in capacity among the cells is a concern for multi-cell operation that might result in significant imbalance and challenge in the cell balancing management. These large disparities in capacity may also arise from the large deviation in internal resistance between cells in this batch.

A summary of the main parameters associated with cell performance variability is presented in Table 3. Concerning the rate capability, the ALT nLTO cells showed larger deviation in variability of rate capability than the SAFT cells, despite what would be expected with the different chemistries of the four cell types. Such variability seems less dependent upon chemistry and more on potential inconsistencies in manufacturing. In terms of capacity ration, the ALT nLTO and the SAFT VL52E high-energy cell designs provide the best consistency. Finally looking at resistance variations, the variations in SAFT VL10VFe are much higher than the observed variations in the ALT nLTO cells. Overall, the cell-to-cell variations of the ALT nLTO cell as well as the SAVL12V and VL52E lies in the acceptable range for BESS applications. The variations of the VL10VFe cell are higher and thus the application of these cells is less recommended.

Table 3. Summary of cell performance variability.

Cell model	Rate capability	Capacity ration	Cell resistance
ALT nLTO	±0.85%	±0.6%	±10%
SAFT VL12V	±0.2%	±1.6%	±6%
SAFT VL52E	±0.2%	±0.6%	±16%
SAFT VL10VFe	±0.4%	±2.8%	±51%

CYCLE LIFE EVALUATION TEST

After the ICCT, one cell of each chemistry was selected for cycle life evaluation. The cycle life evaluation was conducted with a nominal rate of C/3 (full discharge in 3 hours). Contrary to conventional high rate testing, we prefer the mild condition at C/3 for the following reasons: (i) optimizing tester capability and resolution, (ii) allowing calendar aging to play some role in the evaluation process, and (iii) optimizing the data precision and duration of testing to allow detailed capacity fading mechanism analysis for service life prediction.

CYCLE LIFE EVALUATION TEST RESULTS

In this final study, we showcase the cycle aging data for VL12V cell up to 1,400 cycle; for ALT nLTO and VL10VFe cells, 1,350 cycles; and for VL52E cell, 1,100 cycles. These cycle numbers will be referred as end of test (EOT). The variations in cycle numbers among the cells originates from the differences in the recommended charging protocols, which generated variations in the duration of charge regimes. The overall capacity retention results among the cells are summarized in Figure 2.

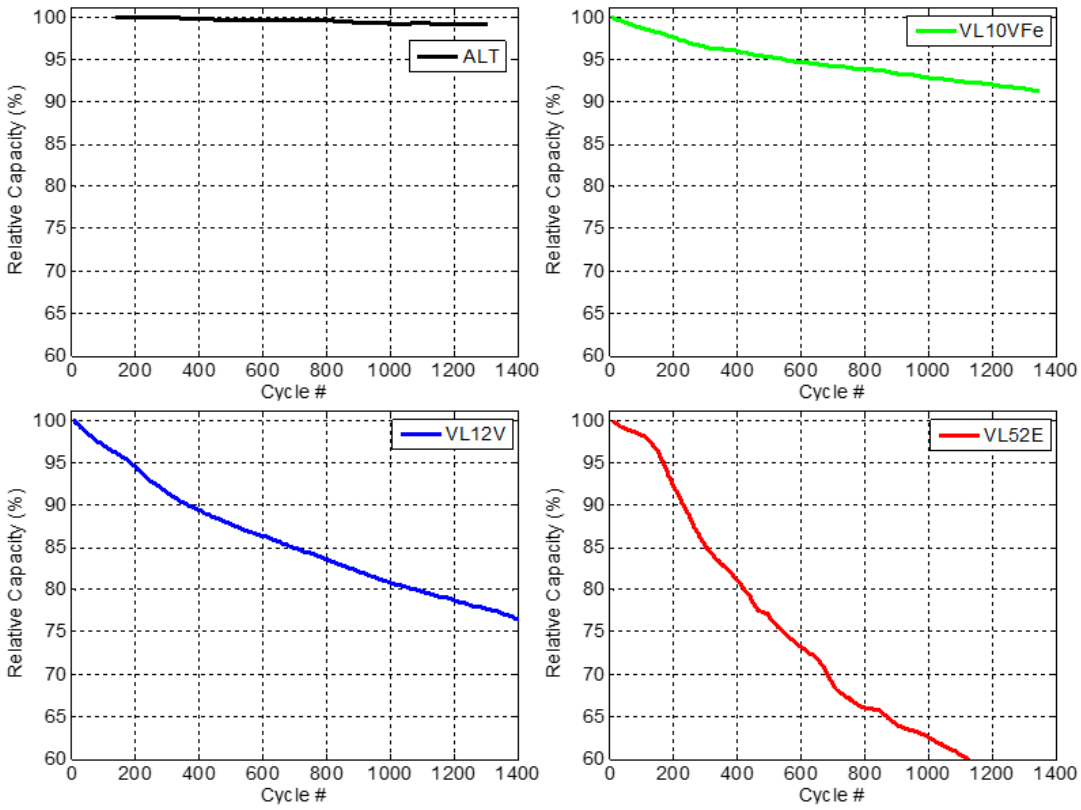

Figure 2: Capacity retention as relative capacity plotted against the number of cycles for the four different cell types subjected to cycle aging experiments.

In Figure 2, the capacity for each cell was normalized to its initial capacity at C/3. In general, the charge retention trend-lines among the four types of cells exhibit a descending pattern in a monotonous manner, indicating that the fading mechanism might remain the same during the entire cycle aging period in each cell type.

Among the four types of cells, the capacity retention exhibited by the ALT cell is the best. The fade rate is on the order of –0.0007% per cycle, which is essentially negligible in 1,400 cycles. The three SA type cells showed more noticeable capacity degradation with various fade rates. The VL10VFe type continued to show a fade rate of –0.0047% per cycle, which is the best among the three and quite constant over the cycle aging so far. The VL52E energy-type cell showed a fade rate of –0.021% per cycle, while the VL12V power-type cell exhibited a fade rate of –0.011% per cycle. It should be noted that for all three SA cells, the rate of capacity fade is decreasing over the cycle aging.

In Figure 3, the capacity fade trend-lines for the four different types of cells are shown for the entire cycle aging evaluation period. The relative changes among the four are compared using a normalized scale to allow visual comparison. For each cell, the capacity measured initially is 100%. After 1,329 cycles of aging, the ALT nLTO cell has retained 99% of its initial capacity. The VL52E cell faded to about 60% of the rated capacity after 1,045 cycles. It passed the end-of-life (EOL), often defined by 80% of the rated capacity, after only 400 cycles. The VL12V cell faded to 76% of the rated capacity after 1,383 cycles, also passed the EOL but this time after 1000 cycles. VL10VFe cell faded to about 91% of its rated capacity after 1,367 cycles. Among the three types of SA cells, this cell retains the best capacity upon cycle aging. It appears that this cell could well pass the 3,000-cycle mark with this fade rate before reaching EOL.

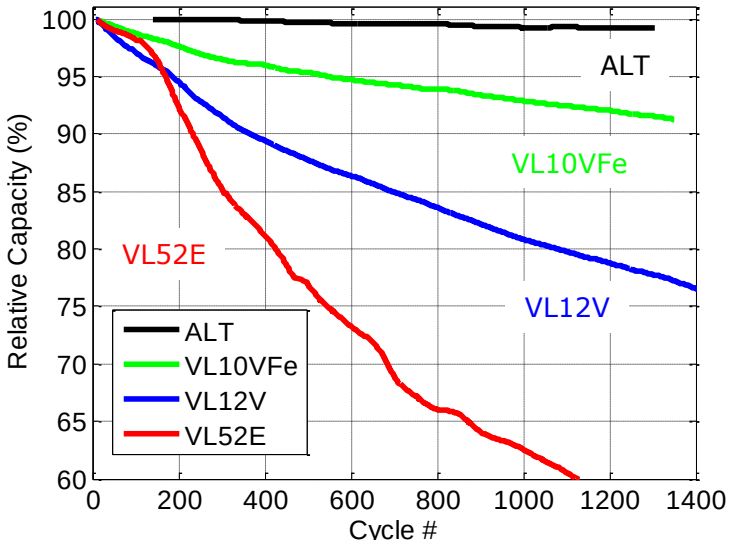

Figure 3: Comparison of the capacity fade rate among the four cell types.

Looking back at Table 1 and the cell chemistries, one can already draw a few interesting conclusions: The ALT nLTO cells suffer almost no degradation compared to the SA cells. This is likely due to the absence of the graphite negative electrode which is known to induce gradual

capacity loss by consuming Li ions while building passivation layers. Among the SA cells, the VL10Fe showcases a slower capacity fade. This was also expected since the LFP positive electrode material is known to be extremely stable upon aging and also because it operates at a lower potential which should limit the growth of the passivation layers. The last two SA cells have the same chemistry but different design (high power vs. high energy). This difference seems to have affected the degradation and the high power cell (VL12V) appears to be more stable.

PROGNOSTIC SIMULATION OF CAPACITY RETENTION

Aiming for further understanding of the capacity fading mechanism and enable prognosis, we conducted detailed analyses using an in-house incremental capacity (dQ/dV) technique. Detailed descriptions of this technique are reported in Refs [2,3,4,5].

The starting hypothesis for our technique is that although the cell is degrading, the electrochemical behavior of each individual electrode is not changing. The capacity loss is then induced by either a change in the balance between the two electrodes (a loss of active material on either side) or a change in the amount of lithium ions that could go back and forth between the electrodes. The data was collected during evaluation following a characterization procedure called reference performance test (RPT), which was performed to obtain the charge retention of the cell at different C/n rates periodically. More precisely, the capacity and power fade of any lithium-ion cell can then be attributed to at least one of five degradation modes: loss of lithium inventory (LLI), loss of active material (LAM) in a lithiated (li) or delithiated (de) state of the positive electrode (PE) or negative electrode (NE) (as denoted by LAM_{dePE}, LAM_{liPE}, LAM_{deNE}, and LAM_{liNE}, respectively). One should be mindful that each cell might have suffered from more than one of these five degradation modes.

Any change in electrode balance and/or lithium content will modify the voltage response of the battery. Studying the changes in the voltage curve upon aging will then provide an insight on the degradation pattern of any cell. Additionally, these variations can be simulated using our in-house model [3] and compared to the experimental values for accurate quantification and prognosis. As the variations can be minute, they are better analyzed by looking at a derivative of the voltage curve: dQ/dV. This technique is known as incremental capacity analysis (ICA).

The contributions from possible degradation modes could vary in proportion as a result of aging conditions. In this work, the aging condition was a constant for all tested cells (C/3 cycling, 25°C

---

2. M. Dubarry, C. Truchot, B.Y. Liaw, "Cell degradation in commercial $LiFePO_4$ cells with high-power and high-energy designs" *J. Power Sources* 258 (2014) 408–419. (doi:10.1016/j.jpowsour.2014.02.052)
3. M. Dubarry, C. Truchot, B.Y. Liaw, "Synthesize battery degradation modes via a diagnostic and prognostic model," *J. Power Sources*, 219 (2012) 204–216. (doi:10.1016/j.jpowsour.2012.07.016)
4 A. Devie, M. Dubarry, B.Y. Liaw, "Overcharge Study in Li4Ti5O12-based Lithium-ion Pouch Cell. Part 1: Quantitative Diagnosis of Degradation Modes." J. Electrochem. Soc, 162(6), p A1033 (2015).
5 M. Dubarry, A. Devie and B. Y. Liaw, "The Value of Battery Diagnostics and Prognostics. "Journal of Energy and Power Sources, 1(5), p. 242-249, (2014), invited paper.

ambient temperature). Therefore, the variation among the cells is primarily the result of cell design and composition of the active materials in response to the aging conditions.

Our in-house model [3], named *'alawa* for the Hawaiian word for "to diagnose", operates by emulating the full cell behavior from half-cell (positive and negative electrode active materials) test data collected from the materials provided by manufacturers or other commercial sources. The half-cell experiments for the ALT nLTO cell were performed in our laboratory as a result of the electrode materials being made available to us. This was the not the case with the SAFT cells since it was unfortunately prohibited under the confidentiality agreement. As a consequence, we had to use alternate half-cell data originating from a source other than SAFT.

The following is the detailed analysis for each cell. We used our expertise in degradation analysis to identify the nature of the degradation mode(s) for each of the test cells. In addition, we intended to establish a quantifiable diagnostic, from the basic mechanisms, not just empirical correlations, from which to enable the prognostic of the cell performance. Such prognostic results need to be validated to support the prediction and to assess if the rate of the degradation from each underlying mechanisms (degradation modes) continue to follow the trend for more accurate extrapolation of the battery life.

ALT nLTO Cell

Figure 4(a) shows the evolution of the charging curves of the ALT nLTO cell from the BOL to EOT, and Figure 4(b) shows the associated dQ/dV curves for the same period.To facilitate discussion, in Figure 4(b), we denoted some of the peak features on the dQ/dV curve in the discharging regime as follows: "A" refers to the region close to the on-set voltage on the voltage-axis from which the peak starts to rise, "B" the absolute intensity (height) of the peak near 2.2 V, "C" the intensity of the "shoulder" of the curve near 2.4–2.5 V, and "D" the region where the peak falls back to the baseline. Using these four markers on the curve to distinguish peak shape variations, we simulated a series of dQ/dV curves from each of the five degradation modes to determine what and how much influence each mode has on these markers. More details on the procedure and this analysis can be found in [4].

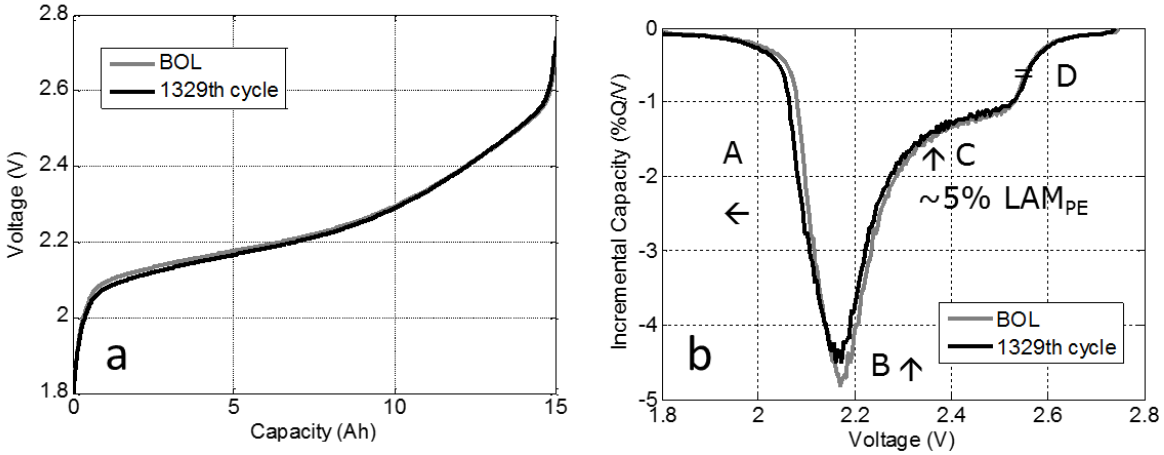

Figure 4 (a): Evolution of discharging curves of the ALT cell from BOL to EOT.
(b): Evolution of the corresponding dQ/dV curves.

As an example of the information obtained from the *'alawa* approach,

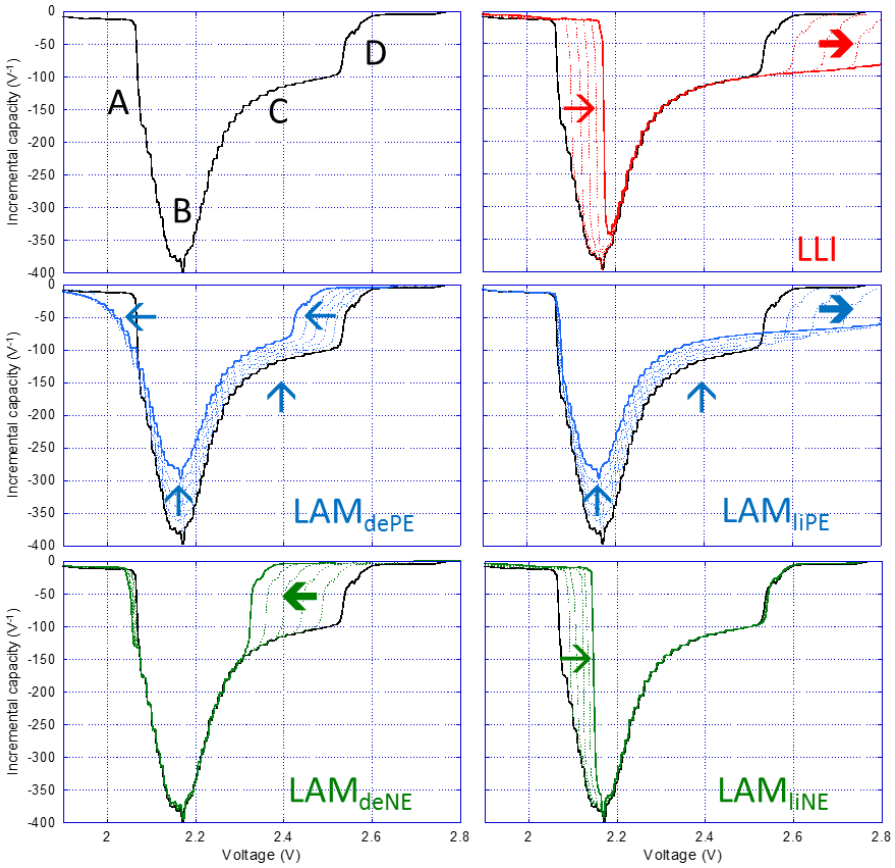

Figure 5 shows the influences of each of the five degradation modes described previously against the dQ/dV curve of the cell at the BOL. Table 4 gives a summary of the observations.

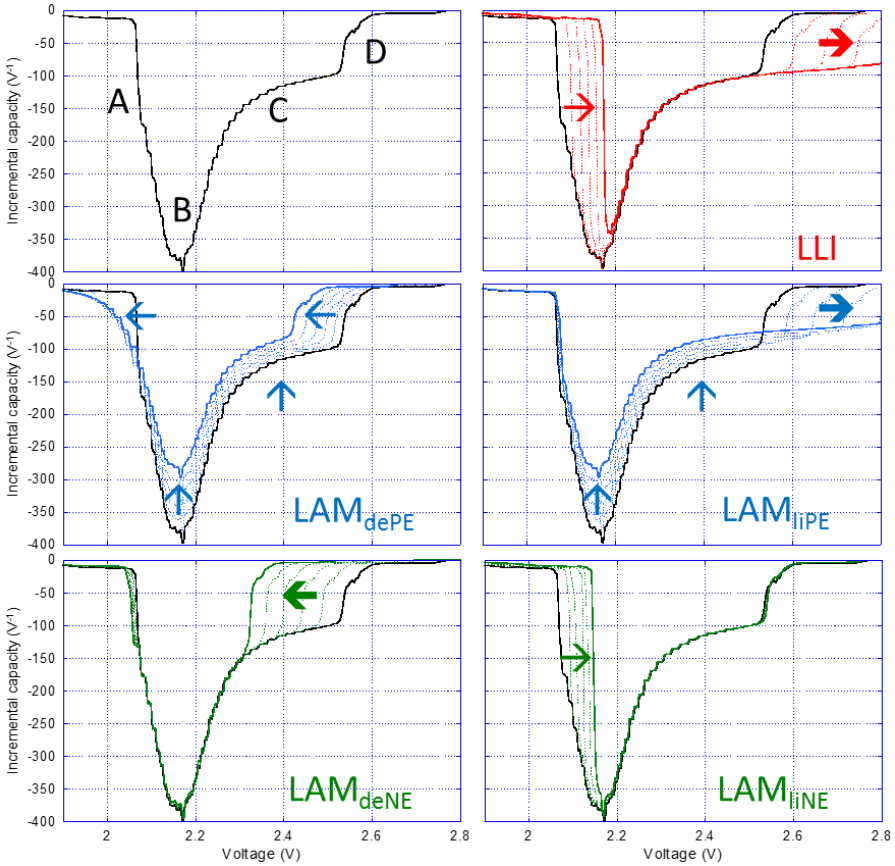

Figure 5: Detailed evolutions of the ABCD regions on the dQ/dV curves of the ALT nLTO cell as a function of the degradation modes.

	A	B	C	D
LLI	→			→
LAM$_{dePE}$	←	↑	↑	←
LAM$_{liPE}$		↑	↑	→
LAM$_{deNE}$				←
LAM$_{liNE}$	→			

Table 4: Summary of the changes in the ABCD regions of the ALT nLTO cell.

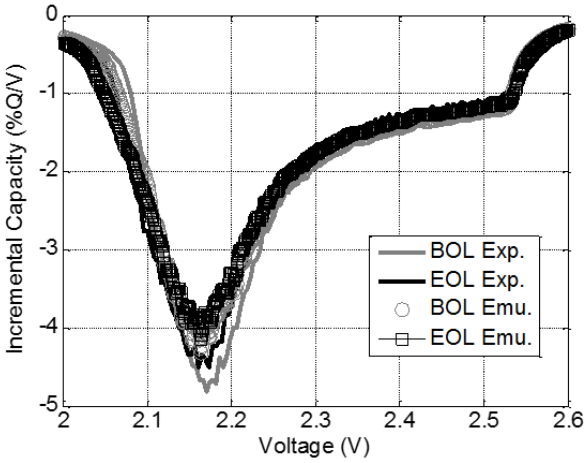

Figure 6: Comparison of the simulated and experimental dQ/dV curves of the ALT cell at the beginning-of-life (BOL) and end-of-life (EOL) with 5% LAM$_{dePE}$ and 1.25% LLI.

On Table 4, the arrows to the right or left direction depict the changes in the dQ/dV peak voltage. The arrows pointed to the up or down directions indicate the changes in the intensity of the dQ/dV peak in the discharge regime.

Using the guide from Table 4 and the evolution highlighted with arrows in Figure 4(b), we found that the changes in the ALT nLTO curve are the result of the combined contributions from LLI and LAM_{dePE}. Indeed, the LAM_{dePE}-induced degradation effects match those observed with A, B, and C markers. Additionally, a small proportion of LLI is required to move the "D" marker to the right, accordingly. In Figure 6, the simulated and experimental dQ/dV curves at the BOL and EOT are compared. Good agreement is reached for a fade that can be attributed to 5% LAM_{dePE} (i.e. 95% of the initial PE capacity remain) and 1.25% LLI (i.e. 98.75% of the initial lithium inventory remain). Using such quantitative information and fade rate, a prognostic emulation can be performed regarding future capacity retention of this ALT nLTO cell under the existing fading mechanism. Indeed, one can extrapolate the rate of LLI and the rate of LAM_{dePE} up to the 10,000 cycles and use the *'alawa* approach to estimate the associated capacity loss. Such a prognosis is shown in Figure 7. The prognosis shows that although the cell faded really slowly up to cycle 1,500, that degradation might accelerate after cycle 3,000 to reach about 30% after 10,000 cycles.

This example showcases the benefit of our approach compared to a simple fit of the capacity loss curve. Indeed, we showed that, even with two linearly fading mechanisms, the associated capacity loss might not be linear and can accelerate. Here, due to the relatively early stage of aging tested for this cell (i.e. 99.0% of its initial capacity retained after 1,300 cycles), there might be a significant level of uncertainty regarding the pace of the LAM_{dePE} and LLI progression. We should caution that the prediction in Figure 7 might be quite premature, and further experimental validation is necessary to corroborate the confidence of the prognostic result.

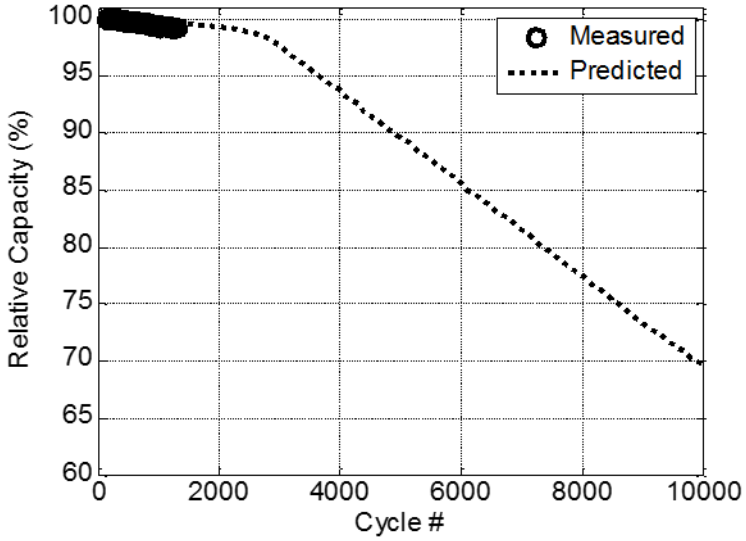

Figure 7: Simulated capacity retention forecast of the ALT cell based on the tested trend of degradation and the contribution of the degradation modes.

In addition to this aging study, a second ALT nLTO cell was tested under different conditions and Figure 8 shows the results of an overcharging event on the ALT nLTO cell during the cycle aging. This is an extremely valuable scenario since overcharging is often considered critical to cell performance and life. In this particular event, the cell was overcharged to 3.6 V which could happen quite often in field operation. The complete analysis of this cell is not in the scope of this report and can be found in an open source publication [4]. In contrast to the main ALT nLTO cell that did not experience any overcharging, this cell showed a very different aging behavior. The analysis showed that the capacity fade resulting from the overcharge came from a combination of degradation modes as a result of LLI (~8%), LAM_{dePE} (~15%), and LAM_{liNE} (~15%).

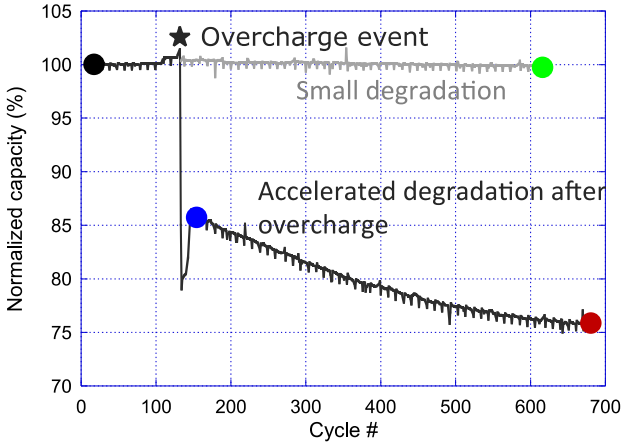

Figure 8: A study of an overcharging event in an ALT cell compared with another ALT cell that was not overcharged (taken from the open source publication [4]).

SA VL10VFe Cell

Using the same diagnostic methodology, we investigated the fading of a SA VL10VFe cell. Figure 9(a) shows the evolution of the charging curves of cell from the BOL to EOT. Figure 9(b) shows the corresponding dQ/dV. Although peak C does not seem to drop in intensity, the area under the peak decreases significantly. This is the proxy we used for diagnosis of the fading mechanism.

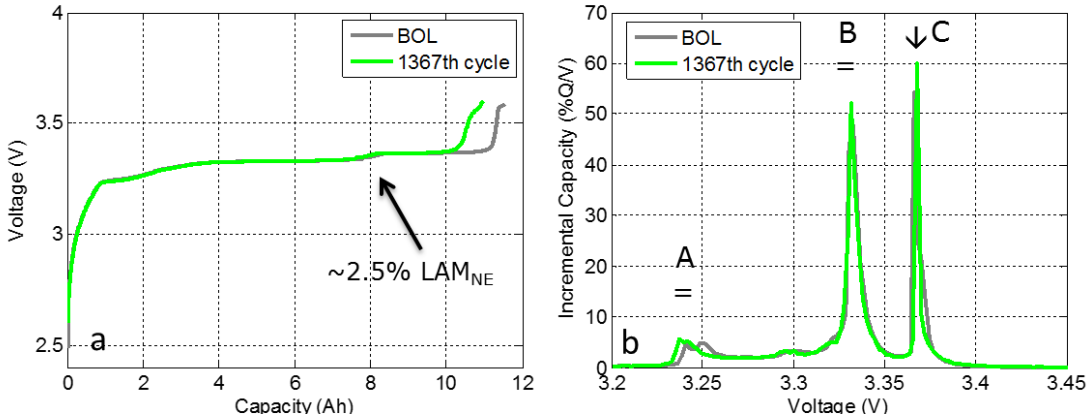

Figure 9: (a) Evolution of the charging curves of an SA VL10VFe cell from BOL to EOT. (b) Evolution of corresponding the dQ/dV curves.

Table 5 summarizes the effects from various degradation modes on the changes of the A, B, and C markers observed in Figure 9(b). From there, we identified that LLI was the degradation mode attributed to the capacity fade in this SA VL10VFe cell. LLI extent is on the order of 8% after nearly 1,400 cycles of aging. From Figure 9 and the estimate of the area under peaks A and B, we were also able to quantify a small contribution of LAM_{NE} on the order of 12.5%. This is not uncommon since, based on experience from other similar studies, we postulated that LLI could result in limited LAM_{NE} as a result of insulation of the ionic pathway in the active grains of graphite [2].

	A	B	C
LLI	=	=	↓
LAM_{dePE}	↓→		
LAM_{liPE}		=→	↓
LAM_{deNE}	↓	↓	↑
LAM_{liNE}	↘	↘	↘

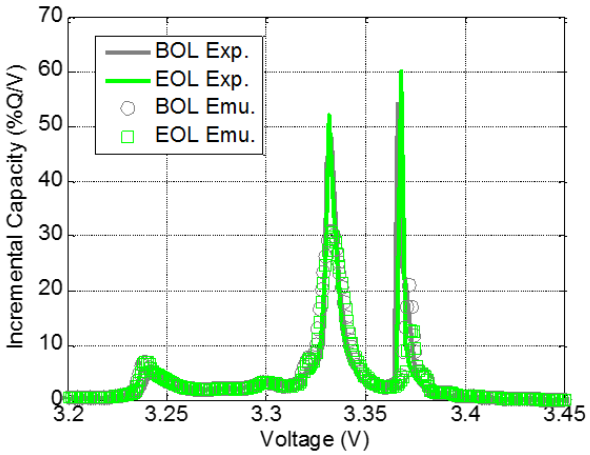

Table 5: Changes in the ABC markers on the dQ/dV curves of the SA VL10VFe cell and Figure 10: Comparison of simulated and experimental dQ/dV curves of the SA VL10VFe cell at the BOL and EOL with 8% LLI and 2.5% LAM_{NE}.

A comparison of the simulated and experimental dQ/dV curves is shown in Figure 10 for the BOL (in gray) and EOT (in green). The consistency in the simulated and experimental results shows good agreement in the understanding of the fading mechanism and the ability to quantify such results. However, it should be noted that the simulated peak shape is different from that of the experimental one. This is due to the fact that the reference active materials in the 'alawa toolbox are likely different to the active materials of the tested cell. The cell design is a high-power type, which often bears a thin electrode configuration. On the other hand, the half-cell data we employed in the model was harvested from a high-energy design. This explains why the simulated dQ/dV curve exhibits peaks with more diffused shape and reduced intensity. However, these minor differences should not compromise the applicability of the diagnostics as the evolution of the dQ/dV curves can be investigated by the variation of the areas under the peaks, which does not change with shape in the analysis [2].

Figure 13 gives a prediction of the capacity retention up to 10,000 cycles based on the projection of the existing degradation modes. Although the tested fade rate after 1,400 cycles is higher than that of the ALT nLTO cell, the projection indicates that the SA VL10VFe cell may retain more than 80% of capacity after more than 8,000 cycles, outperforming the ALT nLTO cell (which showed much less fade after the tested 1400 cycles). After 8000 cycles, we predict that the LAM_{deNE} will become large enough so that lithium plating is likely to occur in the cell which will drastically accelerate the capacity fading. There is always a possibility that a hidden degradation mode may exist that was not detected in the current evaluation period. Such a hidden mode may result in an accelerated capacity fade.

We should be vigilant on such a possibility in the projection's outlook, as it would modify the trajectory of the capacity retention if testing were continued.

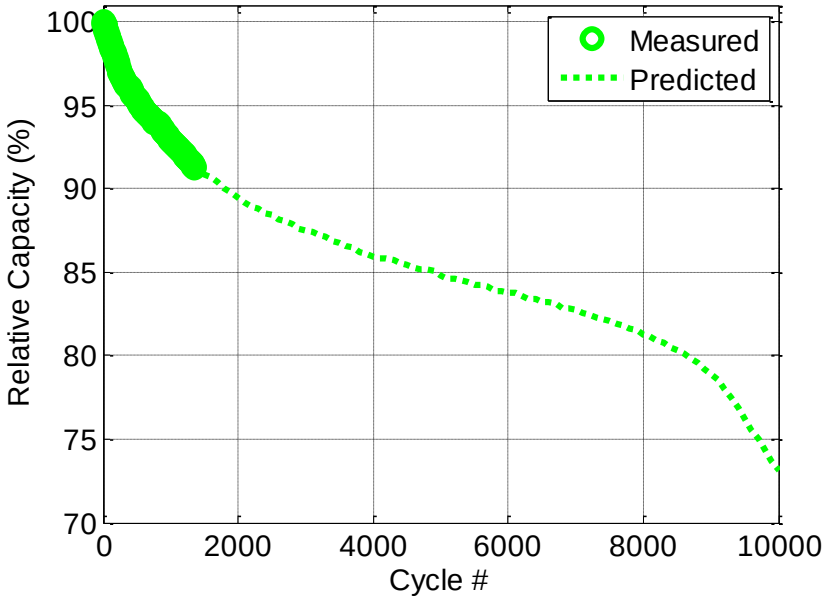

Figure 11: Simulated forecast of the capacity retention in the SA VL10VFe cell based on the existing trend of degradation and the contribution of the degradation modes.

SA VL12V and VL52E Cells

The SA VL12V and VL52E cells share a common chemistry (that uses a graphite negative electrode and NCA positive electrode). They differ in the cell design (i.e. high power vs. high energy, respectively). Here, we discuss the diagnostics of the degradation modes for these two cell types. Figure 12(a) shows the evolution of the charging curves and Figure 12(b) the dQ/dV curves of the SA VL12V cell during the cycle aging experiments.

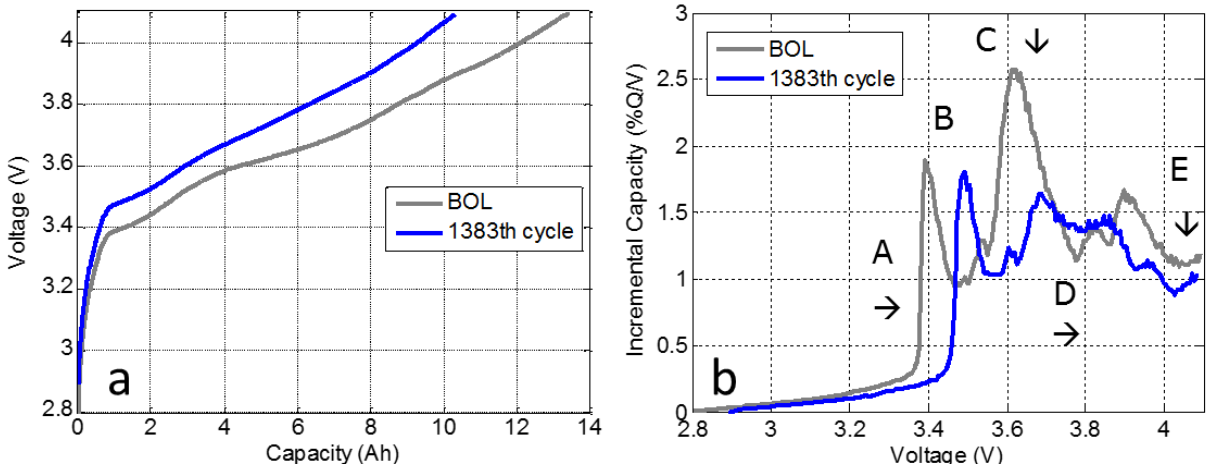

Figure 12: (a) Evolution of the charging curves of the SA VL12V cell from BOL to the end of 1,383 cycles of aging. (b) Evolution of correspondong dQ/dV curves

Table 6 summarizes the effects of degradation modes on the changes of the A, B, C, D, and E markers on the dQ/dV curve as shown in Figure 12(b). The diagnostic analysis showed that LLI (~21%) and LAM_{dePE} (11%) were the degradation modes that contributed to the capacity fade in this VL12V cell. A comparison of the simulated and experimental dQ/dV curves is shown in Figure 13 for the BOL (in gray) and EOT after 1,400 cycles of aging (in blue). This scenario combining LLI and LAM_{dePE} provides overall good agreement on the degradation mechanism in the cycle aging. Again, we observed some inconsistency in the simulated curve from the experimental one in the high voltage region above 3.85 V. Such a discrepancy is likely due to the NCA active material in the SA VL12V cell obtained from the manufacturer being different from the NCA used in the referenced half-cell experiments. We believe the difference does not compromise the diagnosis based on the evolution of the dQ/dV curves. However, it is likely that this difference may affect the accuracy of the quantitative assessment of the degradation. Improved accuracy could be achieved by harvesting the actual positive electrode to generate the half-cell data.

	A	B	C	D	E
LLI	→	↓	↘	→	→
LAMdePE	←	↑	↙	←	↓
LAMliPE	→	↓	↓	→	↓
LAMdeNE	=	↙	←	←	↙
LAMliNE	→	↓=	↘	→	=

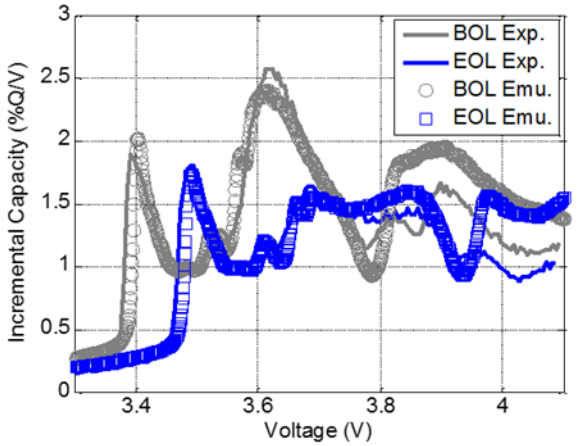

Table 6: Effects of degradation modes on the A, B, C, D, and E markers on the dQ/dV curve of the SA VL12V cell under cycle aging and

Figure 13: Comparison of simulated and experimental dQ/dV curves of the SA VL12V cell at BOL and EOL with a combination of LLI and LAM_{dePE}.

The fading rate of this cell is progressively slowing down with cycle number. Such behavior is commonly encountered with the first few hundred cycles of Li-ion batteries cycling. We took this into account when establishing a forecast based on the contributions from both LLI and LAM_{dePE}. A projection of the capacity retention up to 5,000 cycles based on the existing degradation modes is shown in Figure 14.

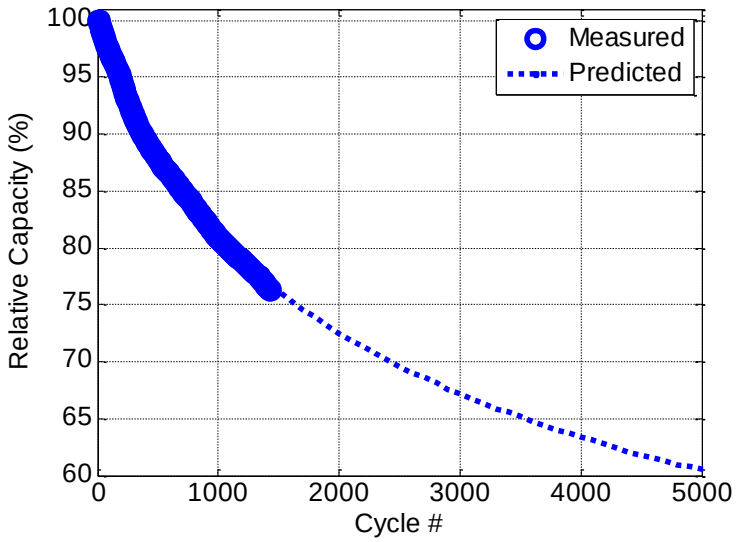

Figure 14: Forecast of capacity retention of the SA VL12V cell based on the existing trend in the degradation and the contribution from the degradation modes.

The SA VL52E cell is a high-energy design. Figure 15(a) shows the evolution of the charging curves and Figure 15 (b) the dQ/dV curves of the SA VL52E cell from the BOL to EOT after 1,000 cycles. Table 7 shows the effects of the degradation modes on the changes of the A, B, C, D, and E markers on the dQ/dV curve shown in Figure 15 (b). Contributions from LAM_{dePE} (~35%) and LLI (~25%) in the capacity fade of the SA VL52E cell were quantified. A comparison of the simulated and experimental dQ/dV curves is shown in Figure 15 for the BOL (in gray) and after 1,000 cycles of aging (in red). The assessment of combining LLI and LAM_{dePE} in the fading mechanism exhibits good agreement with the results between diagnostic simulation and experimental data.

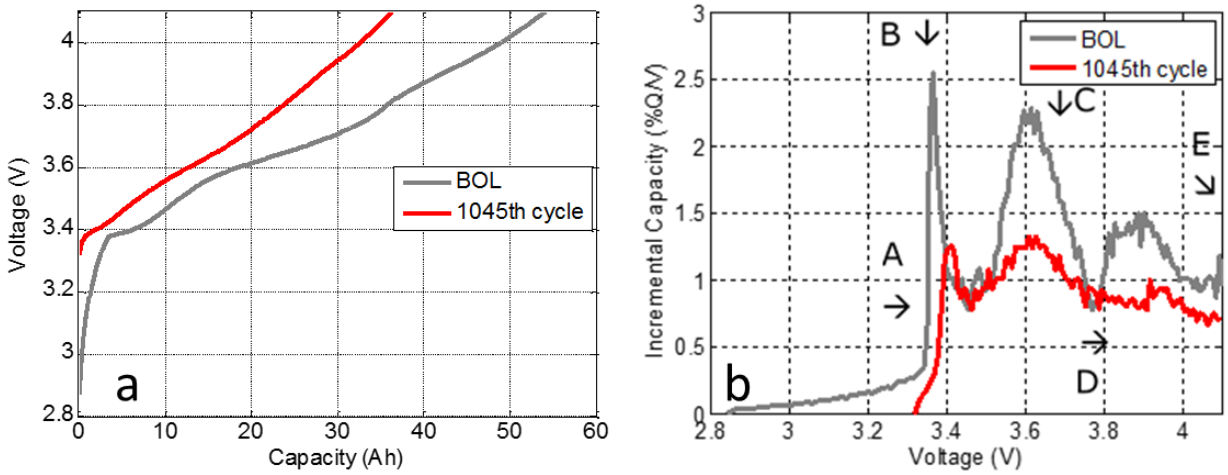

Figure 15: (a) Evolution of the charging curves of the SA VL52E cell through the cycle aging from BOL to the end of 1,045 cycles. (b) Evolution of the dQ/dV curves of the SA VL52E cell from the BOL to the end of 1,045 cycles of aging.

	A	B	C	D	E
LLI	→	↓=	↘	→	→
LAMdePE	←	↑	↙	←	↓
LAMliPE	→	↓	↓	→	↓
LAMdeNE	=	↙	←	←	↙
LAMliNE	→	↓=	↘	→	=

Table 7: Effects of the degradation modes on the changes of the A, B, C, D, and E markers on the dQ/dV curve of the SA VL52E cell through cycle aging.

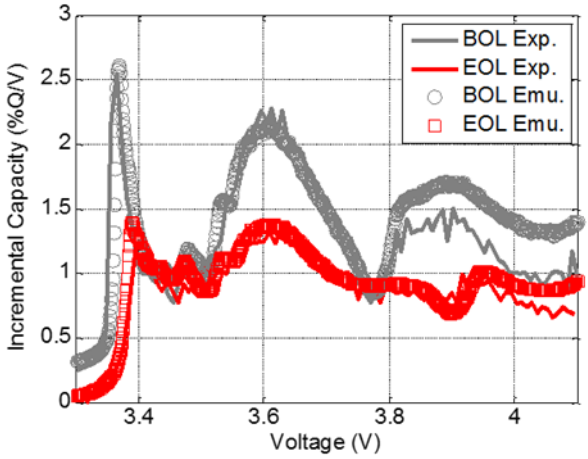

Figure 16: Comparison of the simulated and experimental dQ/dV curves of the SA VL52E cell at the BOL and EOL with a combination of LLI and LAM_{dePE}.

The fading rate of this VL52E cell is also progressively slowing down with cycle number. We took into account of this behavior in establishing the forecast for the cycle life contributed from both LAM_{dePE} and LLI. A projection of the capacity retention up to 2,000 cycles based on the contributions of the existing degradation modes is shown in Figure 17. The discrepancy before the first 100 cycles is probably a result of kinetic effects. With high-energy cell designs, the capacity fade at mid-to-high rates (C/3 is considered a high rate for a high-energy design) is mild in the earlier part of the cycle life due to continuing enhancement of electrode kinetics. The capacity fade at lower rates, on the other hand, shows more immediate fading. This phenomenon has been discussed in one of our earlier works [2].

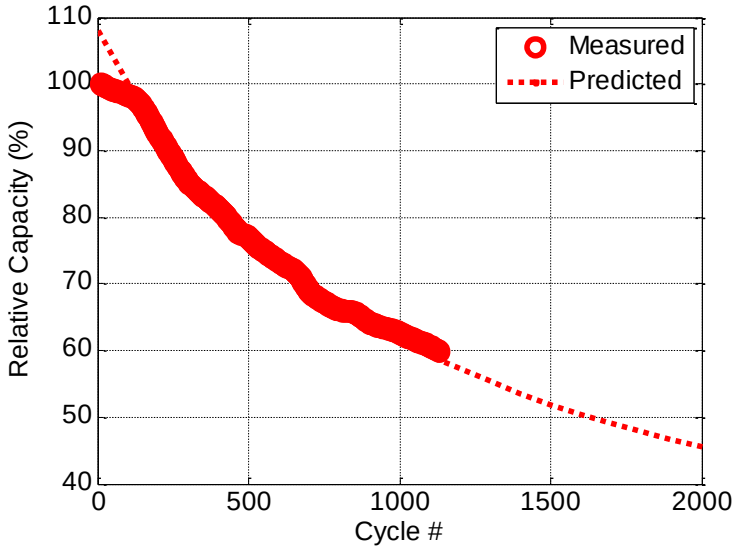

Figure 17: Forecast of capacity retention of the SA VL52E cell based on the existing trend of degradation and the contributions of the degradation modes.

It is interesting to compare the degradation of the VL52E and of the VL12V cells since they are constituted of similar active materials (graphite as the negative and NCA as the positive, cf. Table 1) but differ in design, the VL52E being a high energy cell whereas the VL12V was designed to be a high power cell. Looking at the degradation modes we identified, the high energy cell degradation modes were quantified to be 25% LLI and 35% LAM_{dePE} after 1,000 cycles. For the high energy cell, degradation modes were quantified to be 21% and 11% for LLI and LAM_{dePE} respectively after 1,400 cycles. The LLI is mainly related to the behavior of the negative electrode and the LAM_{dePE} is clearly related to the behavior of the positive electrode. Since the amount of LLI is in the same order of magnitude for both designs, the main difference in the degradation mode can be attributed to the positive electrode. The high energy design, which most likely has larger grains, lower porosity and lower additive content seems more susceptible to loss of active material.

Both cells suffer from LAM_{dePE} and this could explain the observed higher pace of LLI compared to the VL10VFe. Indeed, it is known that if some transition metals are released from the positive electrode, they can poison the negative electrode and accelerate the pace of LLI. This might explain the observed difference between the LFP based cell (VL10VFe) and the NCA based cells (VL12V and VL52E).

CONCLUSIONS

In the course of this study funded by both the DOE Hawai‘i Energy Sustainability Program (HESP) project and ONR funded Hawaii Energy and Environmental Technologies (HEET) 2010 Initiative, we tested four different types of cells, and came to the following conclusions:

1. The ALT nLTO cells showed the least capacity fade (best retention of capacity) of the cells tested in these cycle aging experiments. This is primarily due to the replacement of the graphite (negative) electrode by a more stable lithium titanate oxide (LTO) electrode.

2. Amongst the SAFT cells, the VL10VFe lost the least capacity of the cells tested. It contains an LFP positive electrode whereas the other two SAFT cells contain NCA positive electrode material. LFP is known to be extremely stable upon aging and the cell operates at a lower potential than the other two SAFT cells, which should limit the growth of the passivation layers. The last two SA cells have the same chemistry but different design (high power vs. high energy). The high energy cell (VL52E) degraded faster than the high power cell (VL12V). The high power cell design appears to be more stable. Overall, the most energy dense cell in this study (VL52E) exhibited the worst performance in terms of degradation.

3. The capacity retention projection, based on this study’s test results and prognostic simulation, forecast the best chemistry among the four different types of cells to be the ALT nLTO, closely followed by the SA VL10Fe. Although the SA VL10Fe degraded more during the test, the degradation is forecast to slow down with aging to the 8000^{th} cycle, whereas degradation in the ALT nLTO cell is forecast to accelerate. After the

8000th cycle, the SA VL10Fe is likely to start plating Li-ion and degrade at a faster pace. In any case both should withstanding more than 7,000 cycles at a moderate rate of C/3 in the cycle aging process at room temperature before reaching EOL. The two NCA-based cell designs, either high-energy or high-power, could not last long enough in the cycle aging evaluations for BESS applications. If we consider one full cycle per day for BESS applications, both SA VL10VFe and ALT nLTO cells should be able to provide a service life of about 20 years based on the forecasts. Further testing is needed to validate the projections.

4. It is still too early to tell if additional fading might affect the projection based on existing test data for all cells tested so far. Possible attributes to this uncertainty include:
    a. Electrolyte loss, which is not evaluated from the testing.
    b. Influence of parasitic reactions on the kinetics. , Since the evaluation is too short to tell the consequence of these reactions, the diagnostic from the cannot provide such estimates.
    c. Mechanical failures from the packaging, or other unexpected physical exposure.
    d. Temperature effects and gradients in a large array of multi-cell configurations.
    e. Cell variability.
    f. Incremental overcharging or overdischarging effects.
    g. Overall multi-cell imbalance issues.
    h. Rate and power dependence on the service life.
    i. Self-discharge and the impacts from such behavior.
    j. Other environmental impacts that were not imposed in the tests.
    k. Weather related impacts in field operation.
    l. System control accuracy and power electronics related damage to the cells.
    m. Calendar life due to chemical degradation that is not related to charge transfer.
    n. Blockage of the mass transport over long timeframe of operation that cannot be evaluated in the short test duration we experienced so far.
    o. Electrode durability and integrity.